Inorganic Chemistry

Article

pubs.acs.org/IC

Introducing a New Azoaromatic Pincer Ligand. Isolation and Characterization of Redox Events in Its Ferrous Complexes

Pradip Ghosh,[†] Subhas Samanta,[†,‡] Suman K. Roy,[†] Serhiy Demeshko,[‡] Franc Meyer,[‡] and Sreebrata Goswami[†,*]

[†]Department of Inorganic Chemistry, Indian Association for the Cultivation of Science, Jadavpur, Kolkata 700032, India

[‡]Institut für Anorganische Chemie, Georg-August-Universität Göttingen, Tammannstrasse 4, D-37077 Göttingen, Germany

Supporting Information

ABSTRACT: The isolation and complete characterization of a new bis-azoaromatic ligand, 2,6-bis(phenylazo)pyridine (L), are described, and its coordination to iron(II) is reported. A pseudo-trigonal-bipyramidal mixed-ligand complex of iron(II), $FeLCl_2$ (**1**), and a homoleptic octahedral iron complex, *mer*-$[Fe(L)_2]ClO_4$ $[\mathbf{2}]ClO_4$, have been synthesized from L and $FeCl_2$ or hydrated $Fe(ClO_4)_2$, respectively, in boiling methanol. Determination of the X-ray crystallographic structure together with magnetic data (≈ 5.06 μ_B) and Mössbauer analysis of **1** established a high-spin Fe(II) complex ligated by one neutral 2,6-bis(phenylazo)pyridine ligand. The X-ray crystallographic structure (showing d_{N-N} > 1.30 Å), Mössbauer data, and magnetic susceptibility measurements (≈ 1.65 μ_B) as well as a nearly isotropic EPR signal with only a small metal contribution at g = 1.968, on the other hand, suggest a low-spin Fe(II) complex with a one-electron-reduced radical ligand coordination in $[\mathbf{2}]ClO_4$. The ligand and the metal complexes have well-behaved redox properties, with the ligand(s) functioning as the redox-active site(s) responsible for redox events. The uncoordinated ligand, L, displays a reversible one-electron wave at −1.07 V and a quasi-reversible wave at −1.39 V. The partially reduced ligand $L^{\bullet-}$ shows a single-line EPR spectrum at g = 2.001, signifying that $L^{\bullet-}$ is a free radical. While complex **1** shows a reversible reduction at −0.08 V and an irreversible cathodic response at −0.98 V, the bis-chelate $[\mathbf{2}]ClO_4$ undergoes a reversible one-electron oxidation at 0.54 V and three successive reversible one-electron reductions at −0.18, −0.88, and −1.2 V, all occurring at the ligands without affecting the metal ion oxidation state. The electronic structures of the parent monocationic complex $[\mathbf{2}]^+$ and its oxidized and reduced forms, generated by exhaustive electrolyses, have been characterized by using a host of spectroscopic techniques and density functional theory (DFT). It is found that the 2,6-bis(phenylazo)pyridine ligand (L) is truly redox noninnocent and is capable of coordinating transition-metal centers in its neutral ($[L]^0$), monoanionic monoradical ($[L^{\bullet}]^-$), and dianionic diradical ($[L^{\bullet\bullet}]^{2-}$) forms.

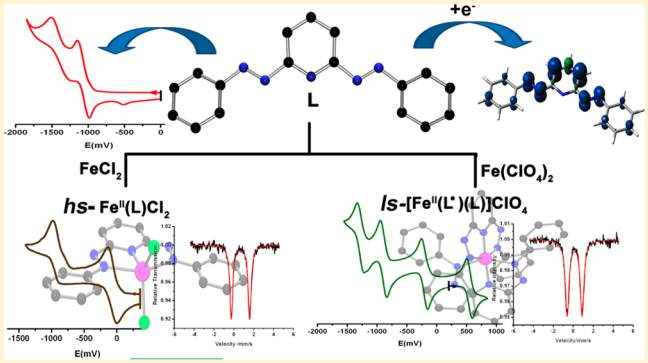

INTRODUCTION

The favorable properties of azoaromatics as redox-active ligands have been quite well substantiated in recent times. This primarily is due to the low-lying π^* orbitals of the coordinated azo function, resulting in multiple electron transfer as a dominant electron sink in their metal complexes.[1,2] For example, six successive redox processes within an accessible range of potentials were noted recently in Rh/Ir complexes[2a,b] of the 2-(arylazo)pyridine ligand. Similar multielectron redox phenomena have been noted in several other complexes of the above and related[3] ligands. In fact, in contemporary research, the studies of redox properties, the isolation of metal complexes in various redox states, and the discovery of different levels of degeneracy[2a,b] in redox series have opened up new possibilities in terms of chemical catalysis and electronic application feasibilities.

Since the azo function in azoaromatics is primarily responsible for the rich redox events in the complexes, the design of suitable ligands containing multiple azo functions is a natural choice for exploration. However, to date, the chemistry of azoaromatics has been dominated by ligands containing a single azo function. As far as we are aware, there is only one example of a bis-azo ligand, viz. 1,3-bis(phenylazo)benzene, whose coordination has been studied for quite some time.[4] However, since it coordinates as an anionic NCN donor and expectedly reductions of its complexes occur at high cathodic potentials, it seems that these are less promising for sequential redox-induced events. Consequently, we have been in search of a neutral ligand that contains multiple reducible azo functions to serve our purpose of multiple redox processes in its complexes. We are further encouraged by a recent report[5] on the superior redox properties of fomazanates over β-diketiminates.

Received: February 13, 2014
Published: April 17, 2014

   dx.doi.org/10.1021/ic500355f | *Inorg. Chem.* 2014, 53, 4678−4686

In this report we wish to disclose the successful isolation of a neutral bis-azo ligand, viz. 2,6-bis(phenylazo)pyridine (L), and its coordination to Fe(II). There is virtually no literature on this ligand except for a German patent[6] describing the use of its 3d ion metal complexes in the rubber-making industry. Furthermore, this ligand has a close resemblance to another tridentate ligand, 2,6-bis(arylimino)pyridine (L′) (Chart 1),

Chart 1

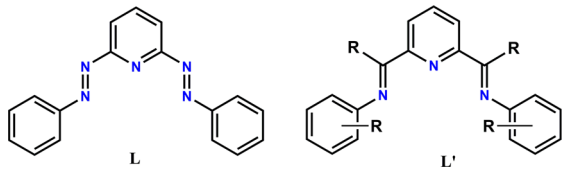

whose coordination chemistry, in general,[7,8] and its redox chemistry, in particular, received a tremendous boost in recent years due to extensive catalytic applications[9,10] of base metal−L′ (Fe and Co in particular) complex catalysts in several useful organic transformations. This indeed is another driving force for taking up the exploration of the coordination chemistry of the reference bis(phenylazo)pyridine ligand with a primary aim of developing, in the long term, potent catalysts[9,10] with synergistic participation of metal and ligand redox activities.

The synthesis and complete characterization of the ligand L and its two iron complexes are the primary concerns of this report. To this end, X-ray crystallography, electrochemistry, and various spectroscopic methods have been applied. Density functional theory (DFT) has been used to address the ambiguity in the oxidation state formalism.

RESULTS AND DISCUSSION

Synthesis. The neutral tridentate ligand L was prepared using a procedure modified from that described for closely related compounds with a single azo group.[11] The synthesis involves condensation of 2,6-diaminopyridine with nitrosobenzene in a 1:2 ratio under highly alkaline conditions. An electrospray ionization (ESI) mass spectrum (MS) of the ligand corroborates its formulation: the ESI MS of L in acetonitrile (see the Supporting Information, Figure S1) displayed a peak at m/z 288 amu for $[L + H]^+$, with the expected isotopic distribution pattern. Its ^{1}H NMR spectrum is shown in Figure 1.

The reactions of L with two ferrous salts, viz. $FeCl_2$ and hydrated $Fe(ClO_4)_2$, at different metal to ligand ratios (Scheme 1) have been studied, and pure material could be isolated in

Scheme 1

$$Fe^{II}Cl_2 + L \xrightarrow{MeOH} Fe^{II}LCl_2\,(\mathbf{1})$$

$$Fe^{II}(ClO_4)_2.6H_2O + 2L \xrightarrow{MeOH} [Fe^{II}(L)(L^{\bullet-})]ClO_4\,([\mathbf{2}]ClO_4)$$

two cases. The reaction between equimolar quantities of $FeCl_2$ and L resulted in a brown crystalline product of composition $FeLCl_2$ (**1**). The reaction between hydrated $Fe(ClO_4)_2$ and 2 equiv of L resulted in a crystalline green product of composition $[Fe(L)_2]ClO_4$ ($[\mathbf{2}]ClO_4$). The ESI MS of the complex $[\mathbf{2}]ClO_4$ in acetonitrile showed an intense peak at m/z 630 amu assigned to $[\mathbf{2}]^+$; its simulated isotopic distribution pattern matched well with the experimental pattern (see the Supporting Information, Figure S2). Elemental analyses (Experimental Section) of the ligand and both complexes corroborate the formulations given above.

Characterization: X-ray Crystallography, Magnetic Susceptibility, and Mössbauer Spectroscopy. The free ligand and its two iron complexes have been characterized using single-crystal X-ray diffraction. Crystallographic details are collected in Table 1, and key bond lengths are compiled in Table 2.

Single crystals suitable for X-ray crystallography of the ligand L were grown by slow evaporation of a dichloromethane solution of the compound. Its ORTEP and atom-numbering scheme are shown in Figure 2. The X-ray crystallographic analysis reveals a planar structure of the free ligand L, with two d_{N-N} values of 1.225(8) and 1.241(8) Å, respectively; these are indicative[12] of double-bond character of the azo functions.

Single crystals of complex **1** suitable for X-ray diffraction analysis were obtained by slow evaporation of its solution in a dichloromethane−hexane solvent mixture. The ORTEP and atom-numbering scheme are shown in Figure 3a. The coordination geometry of complex **1** is best described as a distorted trigonal bipyramid with two N(azo) atoms (N1 and N5) occupying the apical positions with the angle N1−Fe−N5 = 143.53(11)°. The extended azoaromatic ligand and the

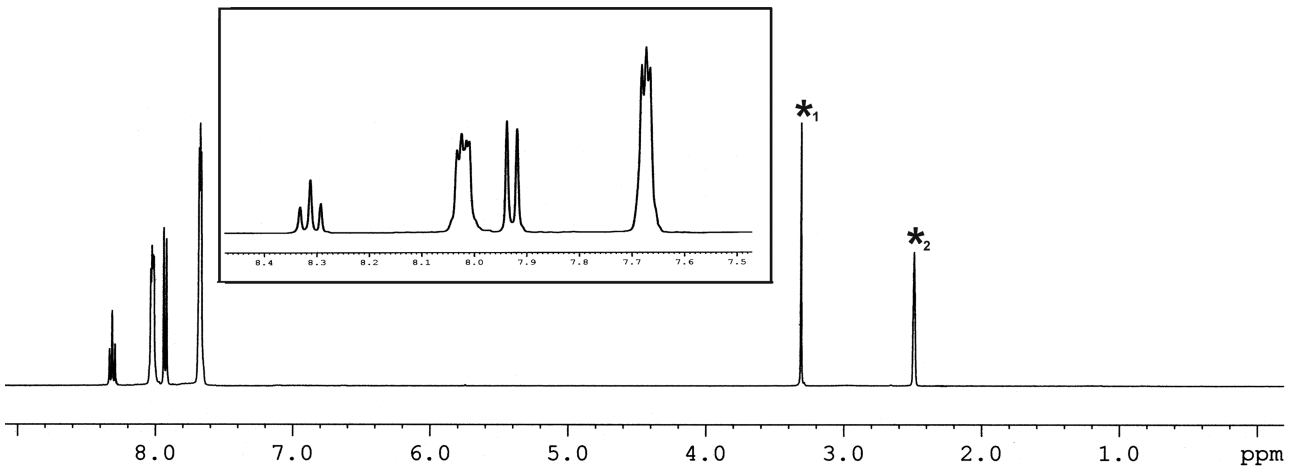

Figure 1. ^{1}H NMR spectrum of L in d_6-DMSO ($*_1$, H_2O; $*_2$, solvent). Inset: aromatic proton resonances.

dx.doi.org/10.1021/ic500355f | Inorg. Chem. 2014, 53, 4678−4686

Table 1. Crystallographic Data for L, 1, and [2]PF_6

	L	1	[2]PF_6
empirical formula	$C_{17}H_{13}N_5$	$C_{17}H_{13}Cl_2FeN_5$	$C_{34}H_{26}FeN_{10}F_6P$
molecular mass (amu)	287.32	414.07	775.47
temp (K)	293	293	293
cryst syst	monoclinic	orthorhombic	orthorhombic
space group	$P2_1/c$	*Pbca*	*Fddd*
a (Å)	6.1995(13)	13.334(2)	14.521(5)
b (Å)	19.910(4)	14.982(3)	27.079(5)
c (Å)	24.478(5)	17.158(3)	32.807(5)
α (deg)	90	90	90
β (deg)	96.343(6)	90	90
γ (deg)	90	90	90
V (Å^3)	3002.9(11)	3427.7(10)	12900(5)
Z	8	8	16
D_{calcd} (g/cm^3)	1.271	1.605	1.597
cryst dimens (mm)	0.12 × 0.15 × 0.17	0.11 × 0.13 × 0.15	0.10 × 0.12 × 0.13
θ range for data collecn (deg)	1.3−17.2	2.4−20.8	1.7−26.5
GOF	1.00	1.05	0.78
no. of rflns collected	12061	19566	40804
no. of unique rflns	1830	1772	3340
final R indices ($I > 2\sigma(I)$)			
R1	0.0363	0.0327	0.0362
wR2	0.0875	0.0851	0.1339

Table 2. Selected Bond Distances (Å) of L, 1, and [2]PF_6

complex	N(1)−N(2)	N(4)−N(5)	Fe(1)−N(1)	Fe(1)−N(3)	Fe(1)−N(5)
L	1.225(8)	1.241(8)			
1	1.283(5)	1.278(4)	2.198(3)	1.995(3)	2.246(3)
[2]PF_6	1.302(3)	1.311(3)	1.971(2)	1.848(2)	1.980(4)

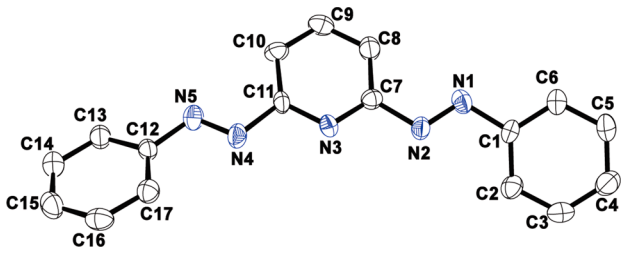

Figure 2. ORTEP of L with ellipsoids at the 30% probability level. Hydrogen atoms are omitted for clarity.

bound metal ion are roughly located in a plane, with no atom deviating by more than 0.04 Å from the mean plane. The d_{N-N} values for the complex are 1.278(4) and 1.283(5) Å, clearly elongated in comparison to those of the free ligand; this may be attributed to the effect of dπ(Fe) → π^*(L) back-bonding interactions.[1a,13]

The perchlorate salt of the cationic complex $[2]^+$ is microcrystalline; however, its hexafluorophosphate salt [2]PF_6 formed crystals suitable for a single-crystal X-ray structure determination. The geometry of the cation $[2]^+$ is a distorted octahedron comprising two meridionally coordinating ligands that orient the two N(py) atoms in mutually trans positions. Its ORTEP and atom-numbering scheme are shown in Figure 3b. Overall the molecule $[2]^+$ has crystallographic C_2 symmetry (noncrystallographic D_{2d} symmetry with an S_4 axis) that makes half of the molecule identical with the other half. In this structure the most significant observation is that the N−N bond lengths are elongated considerably (>1.30 Å), which is taken as an indication that the ligand(s) is (are) reduced[2d] in $[2]^+$. Moreover, the average Fe−N(azo) bond lengths in $[2]^+$ (average 1.975(3) Å) are significantly shorter than those in **1** (average 2.222(3) Å).

The iron complexes are paramagnetic, and variable-temperature magnetic susceptibility measurements were performed on polycrystalline samples of **1** and [2]ClO_4 in the temperature range 295−2 K to confirm the spin states and to assess the magnetic properties of the present systems. The temperature dependence of the magnetic behavior as $\chi_M T$ versus T, χ_M being the molar magnetic susceptibility, is shown in Figure 4. At 295 K, the value of the product $\chi_M T$ for **1** is 3.23 cm^3 mol^{-1} K, which is close to the spin-only value for high-spin Fe(II) with S = 2 (3.00 cm^3 mol^{-1} K). The $\chi_M T$ value of [2]ClO_4 at 295 K is 0.34 cm^3 mol^{-1} K, indicating the presence of one unpaired electron ($S = {}^1/_2$). Data analysis using a fitting procedure to the appropriate spin Hamiltonian for zero-field splitting and Zeeman interaction and including a term for temperature-independent paramagnetism (TIP) provided the values g = 2.07, $|D|$ = 7.1 cm^{-1}, and TIP = 12.8 × 10^{-4} cm^3 mol^{-1} for **1**. The data for [2]ClO_4 were well simulated with g = 2.0 (fixed based on EPR results; see below), TIP = 5.3 × 10^{-4} cm^3 mol^{-1}, and some diamagnetic impurity (DI) of 7.4% (DI had to be included since the g value was fixed at 2.0). The decrease of $\chi_M T$ at temperatures below 10 K could be simulated assuming the Weiss temperature Θ = −3.7 K, which reflects weak intermolecular interactions between radical ligands. Notably, weak intermolecular $\pi-\pi$ interactions can be identified in the solid-state structure of [2]ClO_4.

The electronic structures of **1** and [2]ClO_4 were further authenticated by zero-field ^{57}Fe Mössbauer spectroscopy (Figure 5). The spectrum of **1** at 80 K shows a doublet with isomer shift δ = 0.67 mm/s and quadrupole splitting ΔE_Q = 1.85 mm/s. These values are consistent with the presence of high-spin Fe(II) in a five-coordinate covalent ligand environment.[8i] The isomer shift of **1** is somewhat lower than $\delta \approx 0.9$ mm/s for the related complexes FeL′Cl_2 (L′ = 2,6-bis(arylimino)pyridine),[14] which is in accordance with L being a better π acceptor than L′. For [2]ClO_4 the Mössbauer parameters are δ = 0.14 mm/s and ΔE_Q = 1.49 mm/s, suggesting that the iron(II) ion is in its low-spin d^6 configuration.[8a] Consequently, the spin carrier in the case of [2]ClO_4 should be the radical ligand, with $[Fe^{II}(L)(L^{\bullet-})]^+$ being a reasonable description of the electronic structure. One should note that a much larger quadrupole splitting ΔE_Q would be expected for low-spin iron(III),[8a] and also the N−N bond lengths in $[2]^+$ (d_{N-N} = 1.302(3)/ 1.311(3) Å) are most compatible with an average (caused by crystallographic symmetry) of one neutral L ligand ($d_{N-N} \approx 1.28$ Å) and one singly reduced $L^{\bullet-}$ ligand ($d_{N-N} \approx 1.35$ Å); see Electronic Structure Analysis for further discussion.

Cyclic Voltammetry, EPR, and Spectroelectrochemistry. The redox behavior of the free ligand and its complexes was studied by cyclic voltammetry and related electrochemical techniques; the data are collected in Table 3. The cyclic voltammogram of the ligand L shows two successive one-electron reductions, $[L]^0 \rightarrow [L^{\bullet}]^- \rightarrow [L^{\bullet\bullet}]^{2-}$ at −1.07 and −1.39 V (vs Ag/AgCl), reflecting the sequential filling of the lowest π^* orbitals (Figure 6). Further two-step reduction-

dx.doi.org/10.1021/ic500355f | Inorg. Chem. 2014, 53, 4678−4686

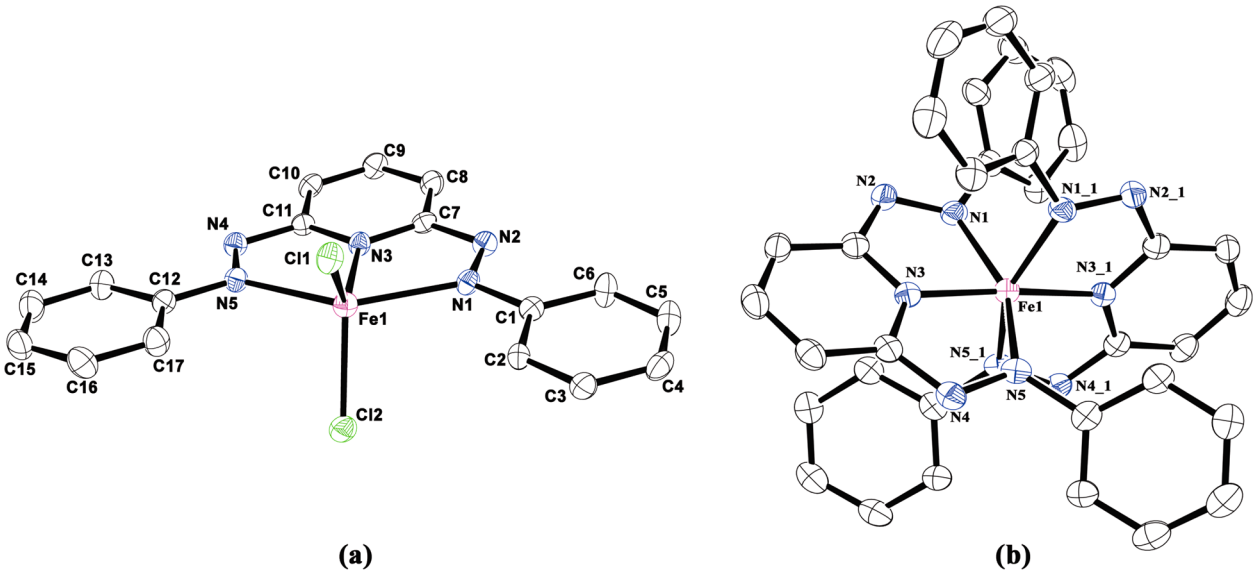

Figure 3. ORTEP of (a) **1** and (b) $[\mathbf{2}]^{+}$ with ellipsoids at the 30% probability level. Hydrogen atoms are omitted for clarity.

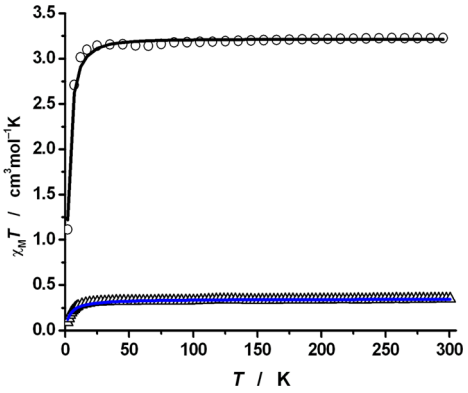

Figure 4. $\chi_M T$ vs T plots of **1** (circles, top) and $[\mathbf{2}]ClO_4$ (triangles, bottom). The solid lines represent the best simulations.

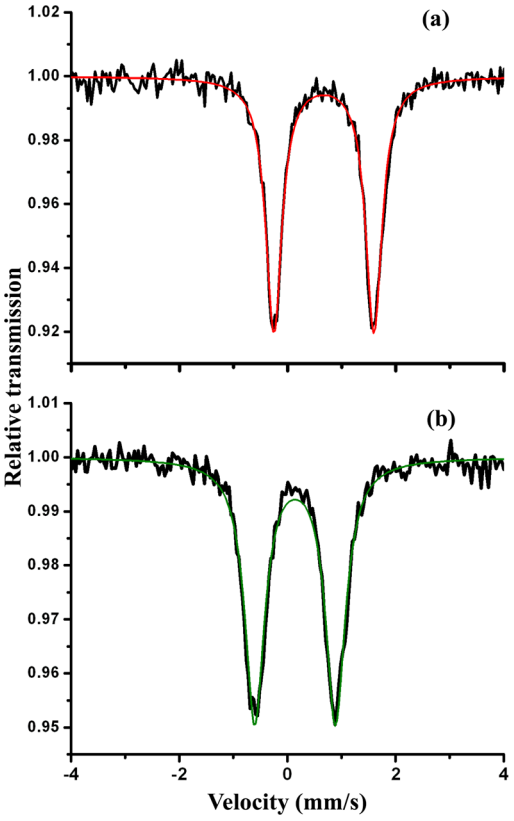

Figure 5. Zero-field ^{57}Fe Mössbauer spectra of (a) **1** and (b) $[\mathbf{2}]ClO_4$ at 80 K. The solid lines represent simulations with Lorentzian doublets.

$s^{2a-d,15}$ to $[L^{\bullet}]^{3-}$ and $[L]^{4-}$, though likely possible, have not been observed under the experimental conditions.

The ligand L can be reduced on the bulk scale by exhaustive electrolysis: the one-electron-reduced product $[L^{\bullet}]^{-}$, generated by partial electrolysis, is green and showed an isotropic EPR signal (g = 2.001) signifying the formation of an anion radical (Figure 7).

This creates a mixed-valent situation within the organic framework with reduction of only one of two azo functions. A low-energy transition was observable at 680 nm. TD-DFT calculations (see below) indicated the two low-energy transitions SOMO(α) → LUMO(α) and SOMO(α) → LUMO+1(α) & LUMO+3(α), in which the SOMO(α) is localized on half of the ligand and the LUMO is localized on the other half. Higher energy orbitals, viz. LUMO+1(α) and LUMO+3(α), have mainly π^* character of the phenyl groups (Supporting Information, Figures S3a and S3b). The calculated lowest energy transition is broad and appeared in the low-energy IR region (outside of our experimental range). However, the absorption at 680 nm observed in our experiment is in the range of the calculated energy (610 nm) for the above transition SOMO(α) → LUMO+1(α) & LUMO+3(α). Visible range spectroelectrochemistry of L showed a gradual generation of $[L^{\bullet}]^{-}$, also evidenced by color changes (Figure 8). The two-electron-reduced product $[L^{\bullet\bullet}]^{2-}$ was hypersensitive, and no meaningful characterization was possible.

Cyclic voltammetry measurements of complexes **1** and $[\mathbf{2}]^{+}$ indicated that, upon coordination of the ligand to Fe(II) in the complexes, the reduction potentials of the azo chromophore underwent considerable anodic shifts. For example, complex **1** shows one reversible reductive response at −0.08 V and an irreversible response at −0.98 V (Figure 6). Exhaustive electrolysis at −0.3 V confirms a one-electron reduction: **1** →

dx.doi.org/10.1021/ic500355f | Inorg. Chem. 2014, 53, 4678−4686

Table 3. Cyclic Voltammetric[a] and UV−Vis Spectral[d] Data of L, 1, and [2]ClO_4

compound	cyclic voltammetry $E_{1/2}$,[b] V (ΔE_p, mV)	UV−vis λ (ε, 10^{-4} M^{-1} cm^{-1})
L	−1.07 (150), −1.39 (200)[c]	440 (0.18), 320 (3.2)
1	−0.08 (100), −0.98[c]	890 (0.1), 540,[e] 410,[e] 335 (1.1)
[2]ClO_4	0.54 (80), −0.18 (80), −0.88 (110), −1.2 (120)	630 (0.39), 415,[e] 340 (3.5)

[a]Conditions: acetonitrile solution for L and **1** (supporting electrolyte $[Et_4N]ClO_4$), dichloromethane solution for complex $[2]^+$ (supporting electrolyte $[Bu_4N]ClO_4$), working electrode platinum, reference electrode Ag/AgCl. [b]$E_{1/2} = 0.5(E_{pa} + E_{pc})$, where E_{pa} and E_{pc} are anodic and cathodic peak potentials, respectively, $\Delta E_p = E_{pa} - E_{pc}$. Scan rate: 50 mV s^{-1}. [c]Quasi-revesible or irreversible. [d]Wavelengths in nm and molar extinction coefficients in M^{-1} cm^{-1}. In acetonitrile solvent for L and **1** and dichloromethane solvent for [2]ClO_4. [e]Shoulder.

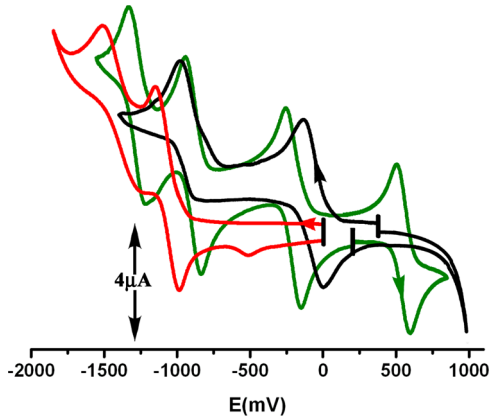

Figure 6. Segmented cyclic voltammograms of L (red), **1** (black), and [2]ClO_4 (green). Conditions: potentials vs Ag/AgCl; L and **1** measured in $CH_3CN/[Et_4N]ClO_4$ solution; $[2]^+$ measured in $CH_2Cl_2/[Bu_4N]ClO_4$ solution.

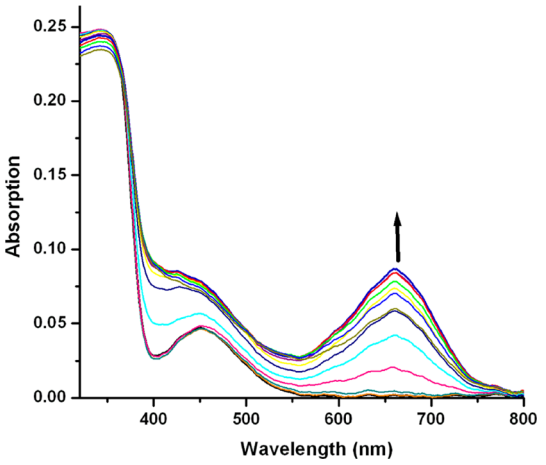

Figure 8. Electronic spectra of gradual generation of the one-electron-reduced ligand $[L^{\bullet}]^-$ in acetonitrile.

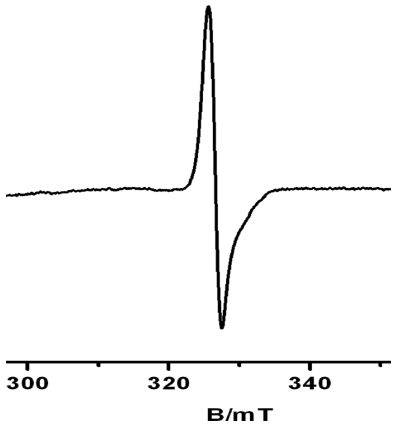

Figure 7. X-band EPR spectrum of $[L^{\bullet}]^-$ in frozen CH_3CN solution at 120 K. Conditions: microwave frequency 9.136 GHz; power 0.998 mW; modulation amplitude 0.1 mT.

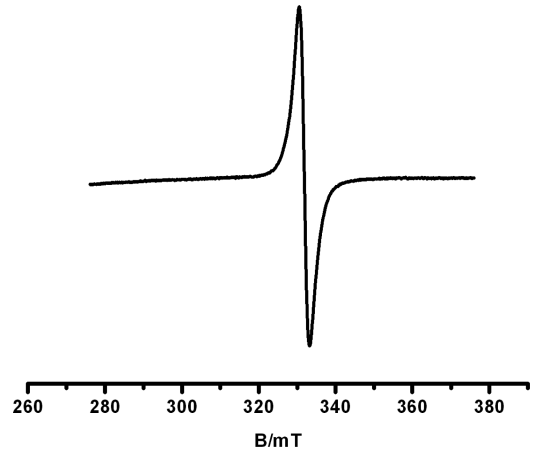

Figure 9. X-band EPR spectrum of $[2]^+$ in frozen CH_2Cl_2 solution at 120 K. Conditions: microwave frequency 9.124 GHz; power 0.998 mW; modulation amplitude 0.1 mT.

$\mathbf{1}^-$. The solution of $\mathbf{1}^-$ is green and showed a broad transition near 660 nm (Supporting Information, Figure S4). The EPR spectrum of coulometrically generated $\mathbf{1}^-$ shows a slightly axial (almost isotropic; see Supporting Information, Figure S5) signal at g = 1.998/1.965, confirming the formation of a radical upon reduction. The anion radical complexes of transition metals are known to often have a slight axial character and g values slightly deviating from 2.0023 due to metal−ligand interactions.[16] $[2]^+$ displayed a nearly isotropic EPR signal with a small metal contribution[16] at g = 1.968 (Figure 9). Accordingly, it is reasonable that unpaired spin resides primarily on the ligands. Unfortunately, however, no ^{14}N hyperfine coupling is observed in the EPR spectrum, either at 120 K or at room temperature. The cationic complex $[2]^+$ thus belongs to a rare class of stable radical complexes. Normally the ligand radical spin in such complexes is quenched via coupling with other unpaired spin(s) within the system.

The cationic complex, $[2]^+$ shows one reversible one-electron oxidation at 0.54 V and three successive reversible one-electron reductions at −0.18, −0.88, and −1.2 V, respectively (Figure 6). The nature of the redox processes in $[2]^+$ was studied by EPR spectroscopy and density functional theory (DFT) calculations (see below). Coulometrically generated oxidized and reduced compounds $[2]^{2+}$ (electrolysis at 0.8 V) and $[2]^0$ (electrolysis at −0.4 V) are EPR silent. The oxidized compound $[2]^{2+}$ was further studied by NMR and Mössbauer spectroscopy. It is diamagnetic and displays a well-resolved ^1H

dx.doi.org/10.1021/ic500355f | Inorg. Chem. 2014, 53, 4678−4686

NMR spectrum; the low number of resonances reflects the high symmetry (D_{2d}) in solution (see the Supporting Information, Figure S6). Its Mössbauer parameters (Supporting Information, Figure S7) are δ = 0.15 mm/s and ΔE_Q = 1.41 mm/s: i.e., very similar to those of parent $[\mathbf{2}]^+$. This suggests that the iron(II) ion remains in its low-spin d^6 configuration. Thus, the results together clearly indicate that the iron center is unaffected and oxidation occurs at the radical ligand center. Since both the oxidized and reduced forms are moderately stable, we have attempted to study their electronic spectral properties, which are depicted in Figure S8 (Supporting Information). Upon oxidation the charge transfer transition at 630 nm of $[\mathbf{2}]^+$ disappeared, while on reduction the band was shifted to the red (20 nm) with augmentation of intensity (Supporting Information, Figure S8). This is an indication[8a] that reduction of the second ligand has occurred in $[\mathbf{2}]^0$, which should thus be described as $[Fe^{II}(L^{\bullet-})_2]^0$. The corresponding bis-ligated iron(II) complex[8a] with 2,6-bis(arylimino)pyridine is diamagnetic and showed a reversible oxidation (assigned to a metal-based Fe(II)/Fe(III) couple) and two reversible one- reductive waves (assigned to ligand-based redox processes) at relatively high potential in comparison to that of complex $[\mathbf{2}]^+$.

Electronic Structure Analysis. In order to have a closer look into the electronic structure of the ligand and complexes, we have performed a series of calculations using DFT at the B3LYP level. The observation that the free ligand L may be reduced by at least two electrons leading to $[L^{\bullet}]^-$ and $[L^{\bullet\bullet}]^{2-}$ with doublet and triplet ground states, respectively, is also evident from the DFT calculations. The calculated geometries and metrical parameters of the ligand in its three oxidation states are collected in Table S1 (Supporting Information). The one-electron-reduced ligand $[L^{\bullet}]^-$ has a doublet ground state (Figure 10), and the net spin density is delocalized primarily

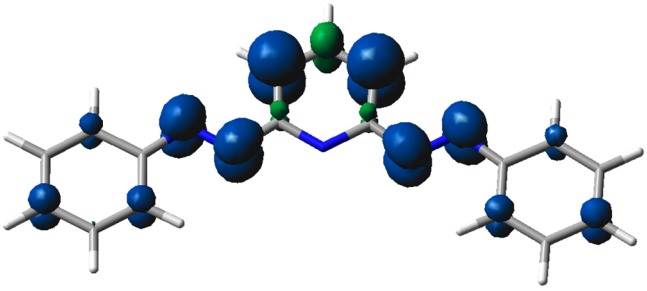

Figure 10. Spin density plot of the one-electron-reduced ligand $[L^{\bullet}]^-$ derived from DFT calculations.

over the pyridyl ring and two azo chromophores. As anticipated, N−N bond lengths of the azo groups are elongated in the reduced ligand (calculated d_{N-N} = 1.292 Å in $[L^{\bullet}]^-$ versus 1.259 Å in L; see the Supporting Information, Table S1).

DFT calculations for the iron complexes considering multiple metal/ligand oxidation or spin state combinations were performed to discount their alternative electronic structures. The observed magnetic moment of the complex **1** is, in principle, consistent with two formulations, including (i) high-spin-Fe^{II} (S_{Fe} = 2) with a neutral ligand (S_L = 0) and (ii) high-spin Fe^{III} (S_{Fe} = $^5/_2$) with one unpaired spin on the ligand (S_L = $^1/_2$) coupled antiferromagnetically, giving rise to the experimentally observed S = 2 ground state description. The latter description is energetically higher than the former by 2.7 kcal/mol. Furthermore, metrical parameters calculated for $Fe^{II}(L)Cl_2$ are in slightly better agreement with experimental values than parameters calculated for $Fe^{III}(L^{\bullet-})Cl_2$. The spin density plot of **1** is shown in Figure 11, and the calculated parameters are collected in Table S2 (Supporting Information). This description is also consistent with its physicochemical behavior (vide supra).

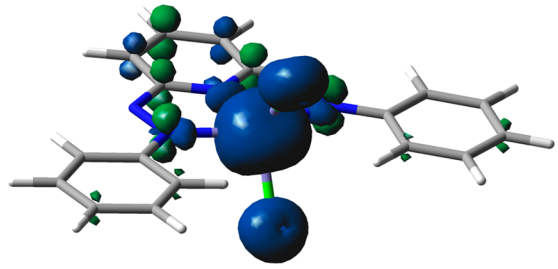

Figure 11. Spin density plot of **1** derived from DFT calculations.

Experimental magnetic data for $[\mathbf{2}]^+$ are consistent with either of the following two formulations: (i) low-spin Fe^{III} (S_{Fe} = $^1/_2$) with two ligand radicals (S_L = +1) and one ligand radical antiferromagnetically coupled to a single metal center spin or (ii) low-spin Fe^{II} (S_{Fe} = 0) and one unpaired electron (S_L = $+^1/_2$) either localized on a single ligand or delocalized over both. DFT calculations for $[\mathbf{2}]^+$ favor a low-spin iron(II) description (Figure 12) for the complex: one unpaired spin is

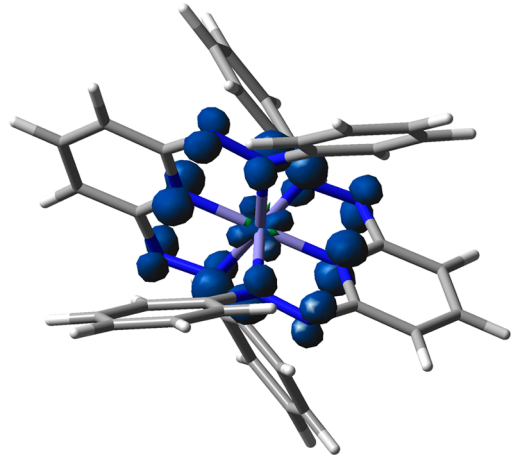

Figure 12. Spin density plot of $[\mathbf{2}]^+$ derived from DFT calculations.

delocalized[17,18] over the two ligands with only a small part (~7%) residing on metal orbitals, which is in line with the observed slight anisotropy in the EPR spectrum of $[\mathbf{2}]^+$. It should be noted, however, that DFT generally has a tendency to overemphasize electron delocalization, and hence a more localized mixed-valent $[Fe^{II}(L)(L^{\bullet-})]^+$ description would be appropriate. The one-electron-reduced compound $[\mathbf{2}]^0$ was optimized in three states: namely singlet closed shell, singlet broken symmetry (BS), and triplet open shell. Among the different optimized structures, the triplet (S = 1) open shell calculated geometry with parallel spin densities (ρ_L = +1.8) on the two ligands is energetically the lowest (Supporting Information, Table S3) and favors a triplet ground state description. Its spin density plot is depicted in Figure S9 (Supporting Information), and the optimized parameters (Table S3) along with Cartesian coordinates are included in the Supporting Information. The difference in calculated

dx.doi.org/10.1021/ic500355f | Inorg. Chem. 2014, 53, 4678−4686

energies between the last two is small (~0.7 kcal/mol). Hence, a triplet description $[Fe(L^{\bullet-})_2]$ appears reasonable and is in accordance with the orthogonal arrangement of the two ligands. Oxidation of $[\mathbf{2}]^+$ is a ligand-based redox process, and the dicationic complex $[\mathbf{2}]^{2+}$ is best described as a low-spin $[Fe^{II}(L)_2]^{2+}$ ($S = 0$) complex, which is consistent with the ^{1}H NMR and Mössbauer spectral data (vide supra).

CONCLUSIONS

In summary, we have introduced the new pincer-type ligand L and the first two metal complexes of that ligand. A major highlight lies in the highly redox noninnocent character of the ligand, which is superior to those of bis(imino)pyridine and related pincer ligands, as anticipated.[7] In particular, L has two easily reducible azo functions that enable the ligand to serve as a multielectron redox reservoir. Thorough crystallographic, spectroscopic, and DFT analysis of two Fe^{II} complexes allowed us to elucidate the coordination mode of L and the electronic structure of the complexes in various overall oxidation states. The new ligand seems far more trivial and readily applicable in comparison to many common systems, and its complexes are expected to have great potential in the growing areas of chemical as well as electronic applications of molecular systems with multiple accessible redox levels. Our efforts in these areas are ongoing and will be reported in due course.

EXPERIMENTAL SECTION

Materials and Measurements. All reagents and chemicals were purchased from commercial sources and used without further purifications. Tetrabutylammonium perchlorate was prepared and recrystallized as reported earlier.[19] *Caution! Perchlorates have to be handled with care and appropriate safety precautions!* Syntheses of the complexes were done in open atmosphere. UV−vis absorption spectra were recorded on a Perkin-Elmer Lambda 950 UV−vis spectrophotometer and a J&M TIDAS instrument. Infrared spectra and NMR spectra were obtained using a Perkin-Elmer 783 spectrophotometer and a Bruker Avance 400/500 MHz spectrometer, respectively, and $SiMe_4$ was used as the internal standard. A Perkin-Elmer 240C elemental analyzer was used to collect microanalytical data (C, H, N). ESI mass spectra were recorded on a Micromass Q-TOF mass spectrometer (Model No. YA263). Cyclic voltammetry potentials were measured under a nitrogen atmosphere using a Ag/AgCl reference electrode, with a Pt-disk working electrode and a Pt-wire auxiliary electrode, in dichloromethane or acetonitrile containing 0.1 M $[Bu_4N]ClO_4$ or 0.1 M $[Et_4N]ClO_4$ respectively. A Pt-gauge working electrode was used for exhaustive electrolyses. The $E_{1/2}$ value for the ferrocenium−ferrocene couple under our experimental conditions was 0.40 V. Mössbauer spectra were recorded with a ^{57}Co source in a Rh matrix using an alternating constant acceleration Wissel Mössbauer spectrometer operated in the transmission mode and equipped with a Janis closed-cycle helium cryostat. Isomer shifts are given relative to iron metal at ambient temperature. Simulation of the experimental data was performed with the Mfit program (E. Bill, Max-Planck Institute for Chemical Energy Conversion, Mülheim/Ruhr, Germany). Temperature-dependent magnetic susceptibility measurements of **1** and $[\mathbf{2}]ClO_4$ were carried out with a Quantum-Design MPMS-XL-5 SQUID magnetometer equipped with a 5 T magnet in the range from 295 to 2.0 K at a magnetic field of 0.5 T for **1** and 0.05 T for $[\mathbf{2}]ClO_4$. The powdered sample was contained in a gel bucket and fixed in a nonmagnetic sample holder. Each raw data file for the measured magnetic moment was corrected for the diamagnetic contribution of the sample holder and the gel bucket. The molar susceptibility data were corrected for the diamagnetic contribution. Temperature-independent paramagnetism (TIP) and a diamagnetic impurity (DI) were included according to $\chi_{calcd} = (1 - DI)\chi + TIP$. Simulation of the experimental magnetic data was performed with the julX program.[20]

Synthesis. *Preparation of L.* The ligand, L was synthesized[11] and purified by following a procedure slightly modified from that for 2-(phenylazo)pyridine, with 2,6-diaminopyridine was used in place of 2-aminopyridine in a 1:2 molar proportion. Yield: 30%. IR (KBr, cm^{-1}): 1571 (ν(C═N) + ν(C═C)), 1448 (ν(N═N)). Anal. Calcd for $C_{17}H_{13}N_5$: C, 71.06; H 4.56; N 24.37. Found: C, 70.94; H, 4.80; N, 23.98. ESI-MS: m/z 288 $[M + H]^+$. ^{1}H NMR (d_6-DMSO, 400 MHz): 8.31 (t, 1H, J = 7.6 Hz), 8.03−8.00 (m, 4H), 7.92 (d, 2H, J = 7.6 Hz), 7.67 (t, 6H, J_1 = 3.6 Hz, J_2 = 2.8 Hz) ppm.

*Preparation of $FeLCl_2$ (**1**).* A mixture of 126 mg (1 mmol) of $FeCl_2$ and 287 mg (1 mmol) of L in 50 mL of methanol was refluxed for 4 h. The resulting brown solution was evaporated to dryness. The crude residue was subsequently extracted with dichloromethane and recrystallized from dichloromethane−hexane solution. Yield: 91% (375 mg). IR (KBr, cm^{-1}): 1580 (ν(C═N) + ν(C═C)), 1430 (ν(N═N)). Anal. Calcd for $C_{17}H_{13}Cl_2FeN_5$: C, 49.31; H, 3.16; N, 16.91. Found: C, 49.74; H, 3.20; N, 17.12.

Preparation of $Fe(L)_2ClO_4$ ($[\mathbf{2}]ClO_4$). A mixture of 180 mg (0.5 mmol) of $Fe(ClO_4)_2{\cdot}6H_2O$ and 287 mg (1 mmol) of L in 50 mL of methanol was refluxed for 3 h. The resulting green solution was evaporated to dryness. The crude residue was subsequently extracted with dichloromethane and recrystallized from dichloromethane−hexane solution. Yield: 78% (285 mg). IR (KBr, cm^{-1}): 1580 (ν(C═N) + ν(C═C)), 1350 (ν(N═N)). Anal. Calcd for $C_{34}H_{26}FeN_{10}ClO_4$: C, 55.95; H, 3.59; N, 19.19; Found: C, 55.53; H, 3.59; N, 19.13. ESI-MS: m/z 630 $[\mathbf{2}]^+$. The corresponding hexafluorophosphate salt, $[\mathbf{2}]PF_6$, was obtained in >90% yield by the addition of a saturated aqueous solution of $[NH_4]PF_6$ to a solution of $[\mathbf{2}]ClO_4$ in methanol.

X-ray Crystallography. Crystallographic data for compounds L, **1**, and $[\mathbf{2}]PF_6$ are collected in Table 1. Suitable X-ray-quality crystals of these compounds were obtained by the slow evaporation of a dichloromethane−hexane solution of the compound. All data were collected on a Bruker SMART APEX-II diffractometer, equipped with graphite-monochromated Mo Kα radiation (λ =0.71073 Å), and were corrected for Lorentz polarization effects.

L: a total of 12061 reflections were collected, of which 1830 were unique (R_{int} = 0.062), satisfying the $I > 2\sigma(I)$ criterion, and were used in subsequent analysis.

1: a total of 19566 reflections were collected, of which 1772 were unique (R_{int} = 0.108), satisfying the $I > 2\sigma(I)$ criterion, and were used in subsequent analysis.

$[\mathbf{2}]PF_6$: a total of 40804 reflections were collected, of which 3340 were unique (R_{int} = 0.04).

The structures were solved by employing the SHELXS-97 program package[21] and were refined by full-matrix least squares based on F^2 (SHELXL-97).[22] All hydrogen atoms were added in calculated positions.

Computational Details. All DFT calculations presented in this paper were carried out using the Gaussian 09W program package.[23] Full geometry optimizations were performed without symmetry constraints. The vibrational frequency calculations were performed to ensure that the optimized geometries represent the local minima and that there are only positive eigenvalues. The hybrid B3LYP exchange-correlation functional[24] was used. The TZVP basis set[25] of triple-ζ quality with one set of polarization functions was used on Fe and Cl atoms, and the 6-31G(d) basis set was used for the C, H, and N atoms. The broken-symmetry approach[26,27] was employed to establish the singlet state $S = 0$ of the compound(s). The calculations of the ground-state singlet states were performed using either spin-restricted or spin-unrestricted approaches (in G09W, combined with GUESS=MIX). Mulliken spin densities were used for analysis of the spin populations on ligand and metal centers.[28] Singlet excitation energies based on the solvent-phase (CH_3CN) optimized geometry of the compound L were computed using the time-dependent density functional theory (TDDFT) formalism[29] in acetonitrile using the conductor-like polarizable continuum model.[30] GaussSum[31] was used to calculate the percentage contribution of ligand and metal to the frontier orbital and the fractional contributions of various molecular orbitals in the optical spectral transition.

dx.doi.org/10.1021/ic500355f | Inorg. Chem. 2014, 53, 4678−4686

■ ASSOCIATED CONTENT

Supporting Information

Figures, tables, and CIF files giving ESI-MS spectra of L and $[\mathbf{2}]^+$, orbitals involved in the electronic transition of $[L^{\bullet}]^-$. electronic spectra of **1** and $\mathbf{1}^-$, EPR spectrum of the electrogenerated reduced complex $\mathbf{1}^-$, ^{1}H NMR spectrum of the electrogenerated oxidized compound $[\mathbf{2}]^{2+}$, Mössbauer spectrum of the electrogenerated oxidized compound $[\mathbf{2}]^{2+}$, electronic spectra of $[\mathbf{2}]^+$, $[\mathbf{2}]^{2+}$, and $[\mathbf{2}]^0$, spin density plots of the one-electron-reduced compound $[\mathbf{2}]^0$ and the two-electron-reduced ligand $(L^{\bullet\bullet})^{2-}$, frontier molecular orbitals of the oxidized complex $[\mathbf{2}]^{2+}$, selected experimental and calculated bond distances for L, $[L^{\bullet}]^-$ and $[L^{\bullet\bullet}]^{2-}$, selected experimental and calculated bond parameters for **1**, $[\mathbf{2}]^+$, $[\mathbf{2}]^{2+}$, and $[\mathbf{2}]^0$, Cartesian coordinates of the optimized structures of $[\mathbf{2}]^+$, $[\mathbf{2}]^{2+}$, and $[\mathbf{2}]^0$, and crystallographic data for L, **1**, and $[\mathbf{2}]PF_6$. This material is available free of charge via the Internet at http://pubs.acs.org.

■ AUTHOR INFORMATION

Corresponding Author

*E-mail: icsg@iacs.res.in.

Notes

The authors declare no competing financial interest.

■ ACKNOWLEDGMENTS

Financial support received from the Department of Science and Technology (Project SR/S1/IC/0031/2010), New Delhi, India, is acknowledged. S.G. thanks the DST for a J. C. Bose fellowship. Crystallography was performed at the DST funded National Single Crystal Diffractometer Facility at the Department of Inorganic Chemistry, IACS. P.G. and S.K.R. thank the Council of Scientific and Industrial Research for fellowship support. S.S. thanks the Alexander von Humboldt foundation for a postdoctoral fellowship.

■ REFERENCES

(1) (a) Ghosh, B. K.; Chakravorty, A. *Coord. Chem. Rev.* **1989**, *95*, 239−294. (b) Kaim, W. *Inorg. Chem.* **2011**, *50*, 9752−9765. (c) Sarkar, B.; Patra, S.; Fiedler, J.; Sunoj, R. B.; Janardana, D.; Mobin, S. M.; Niemeyer, M.; Lahiri, G. K.; Kaim, W. *Angew. Chem., Int. Ed.* **2005**, *44*, 5655−5658. (d) Sarkar, B.; Patra, S.; Fiedler, J.; Sunoj, R. B.; Janardanan, D.; Lahiri, G. K.; Kaim, W. *J. Am. Chem. Soc.* **2008**, *130*, 3532−3542. (e) Kaim, W. *Coord. Chem. Rev.* **2001**, *219*−*221*, 463−488. (f) Doslik, N.; Sixt, T.; Kaim, W. *Angew. Chem., Int. Ed.* **1998**, *37*, 2403−2404.

(2) (a) Goswami, S.; Sengupta, D.; Paul, N. D.; Mondal, T. K.; Goswami, S. *Chem. Eur. J.* **2014**, DOI: 10.1002/chem.201304369. (b) Paul, N. D.; Rana, U.; Goswami, S.; Mondal, T. K.; Goswami, S. *J. Am. Chem. Soc.* **2012**, *134*, 6520−6523. (c) Ghosh, P.; Samanta, S.; Roy, S. K.; Joy, S.; Krämer, T.; McGrady, J. E.; Goswami, S. *Inorg. Chem.* **2013**, *52*, 14040−14049. (d) Samanta, S.; Ghosh, P.; Goswami, S. *Dalton Trans.* **2012**, *41*, 2213−2226. (e) Joy, S.; Krämer, T.; Paul, N. D.; Banerjee, P.; McGrady, J. E.; Goswami, S. *Inorg. Chem.* **2011**, *50*, 9993−10004. (f) Paul, N.; Samanta, S.; Goswami, S. *Inorg. Chem.* **2010**, *49*, 2649−2655. (g) Sanyal, A.; Chatterjee, S.; Castiñeiras, A.; Sarkar, B.; Singh, P.; Fiedler, J.; Záliš, S.; Kaim, W.; Goswami, S. *Inorg. Chem.* **2007**, *46*, 8584−8593. (h) Sanyal, A.; Banerjee, P.; Lee, G.-H.; Peng, S.-M.; Hung, C.-H.; Goswami, S. *Inorg. Chem.* **2004**, *43*, 7456−7462. (i) Samanta, S.; Singh, P.; Fiedler, J.; Záliš, S.; Kaim, W.; Goswami, S. *Inorg. Chem.* **2008**, *47*, 1625−1633.

(3) (a) Luca, O. R.; Crabtree, R. H. *Chem. Soc. Rev.* **2013**, *42*, 1440−1459. (b) Dzik, W. I.; van der Vlugt, J. I.; Reek, J. N. H.; de Bruin, B. *Angew. Chem., Int. Ed.* **2011**, *50*, 3356−3358. (c) Enright, D.; Gambarotta, S.; Yap, G. P. A.; Budzelaar, P. H. M. *Angew. Chem., Int. Ed.* **2002**, *41*, 3873−3876. (d) Praneeth, V. K. K.; Ringenberg, M. R.; Ward, T. R. *Angew. Chem., Int. Ed.* **2012**, *51*, 10228−10234. (e) Lu, C. C.; Bill, E.; Weyhermüller, T.; Bothe, E.; Wieghardt, K. *J. Am. Chem. Soc.* **2008**, *130*, 3181−3197.

(4) Majumder, P.; Baksi, S.; Halder, S.; Tadesse, H.; Blake, A. J.; Drew, M. G. B.; Bhattacharya, S. *Dalton Trans.* **2011**, *40*, 5423−5425 and referenecs therein.

(5) Chang, M.-C.; Dann, T.; Day, D. P.; Lutz, M.; Wildgoose, G. G.; Otten, E. *Angew. Chem., Int. Ed.* **2014**, *53*, 4118−4122.

(6) Kerns, M. L.; Bowen, D. E., III; Rodewald, S. German Pat. Appl. DE 10038214 A1, 2000.

(7) Zhu, D.; Budzelaar, P. H. M. *Organometallics* **2008**, *27*, 2699−2705.

(8) (a) de Bruin, B.; Bill, E.; Bothe, E.; Weyhermüller, T.; Wieghardt, K. *Inorg. Chem.* **2000**, *39*, 2936−2947. (b) Budzelaar, P. H. M.; de Bruin, B.; Gal, A. W.; Wieghardt, K.; van Lenthe, J. H. *Inorg. Chem.* **2001**, *40*, 4649−4655. (c) Stieber, S. C. E.; Milsmann, C.; Hoyt, J. M.; Turner, Z. R.; Finkelstein, K. D.; Wieghardt, K.; DeBeer, S.; Chirik, P. J. *Inorg. Chem.* **2012**, *51*, 3770−3785. (d) Bowman, A. C.; Milsmann, C.; Bill, E.; Turner, Z. R.; Lobkovsky, E.; DeBeer, S.; Wieghardt, K.; Chirik, P. J. *J. Am. Chem. Soc.* **2011**, *133*, 17353−17369. (e) Bowman, A. C.; Milsmann, C.; Bill, E.; Lobkovsky, E.; Weyhermüller, T.; Wieghardt, K.; Chirik, P. J. *Inorg. Chem.* **2010**, *49*, 6110−6123. (f) Bowman, A. C.; Milsmann, C.; Atienza, C. C. H.; Lobkovsky, E.; Wieghardt, K.; Chirik, P. J. *J. Am. Chem. Soc.* **2010**, *132*, 1676−1684. (g) Wile, B. M.; Trovitch, R. J.; Bart, S. C.; Tondreau, A. M.; Lobkovsky, E.; Milsmann, C.; Bill, E.; Wieghardt, K.; Chirik, P. J. *Inorg. Chem.* **2009**, *48*, 4190−4200. (h) Bart, S. C.; Lobkovsky, E.; Bill, E.; Wieghardt, K.; Chirik, P. J. *Inorg. Chem.* **2007**, *46*, 7055−7063. (i) Bart, S. C.; Chłopek, K.; Bill, E.; Bouwkamp, M. W.; Lobkovsky, E.; Neese, F.; Wieghardt, K.; Chirik, P. J. *J. Am. Chem. Soc.* **2006**, *128*, 13901−13912. (j) Darmon, J. M.; Turner, Z. R.; Lobkovsky, E.; Chirik, P. J. *Organometallics* **2012**, *31*, 2275−2285.

(9) (a) Chirik, P. J.; Wieghardt, K. *Science* **2010**, *327*, 794−795. (b) Tondreau, A. M.; Atienza, C. C. H.; Weller, K. J.; Nye, S. A.; Lewis, K. M.; Delis, J. G. P.; Chirik, P. J. *Science* **2012**, *335*, 567−570. (c) Hoyt, J. M.; Sylvester, K. T.; Semproni, S. P.; Chirik, P. J. *J. Am. Chem. Soc.* **2013**, *135*, 4862−4877. (d) Russell, S. K.; Lobkovsky, E.; Chirik, P. J. *J. Am. Chem. Soc.* **2011**, *133*, 8858−8861. (d) Obligacion, J. V.; Semproni, S. P.; Chirik, P. J. *J. Am. Chem. Soc.* **2014**, *136*, 4133−4136. (e) Obligacion, J. V.; Chirik, P. J. *J. Am. Chem. Soc.* **2013**, *135*, 19107−19110. (f) Obligacion, J. V.; Chirik, P. J. *Org. Lett.* **2013**, *15*, 2680−2683. (g) Hoyt, J. M.; Sylvester, K. T.; Semproni, S. P.; Chirik, P. J. *J. Am. Chem. Soc.* **2013**, *135*, 4862−4877. (h) Yu, R. P.; Darmon, J. M.; Hoyt, J. M.; Margulieux, G. W.; Turner, Z. R.; Chirik, P. J. *ACS Catal.* **2012**, *2*, 1760−1764. (i) Monfette, S.; Turner, Z. R.; Semproni, S. P.; Chirik, P. J. *J. Am. Chem. Soc.* **2012**, *134*, 4561−4564. (j) Russell, S. K.; Lobkovsky, E.; Chirik, P. J. *J. Am. Chem. Soc.* **2011**, *133*, 8858−8861. (k) Atienza, C. C. H.; Milsmann, C.; Lobkovsky, E.; Chirik, P. J. *Angew. Chem., Int. Ed.* **2011**, *50*, 8143−8147. (l) Russell, S. K.; Lobkovsky, E.; Chirik, P. J. *J. Am. Chem. Soc.* **2011**, *133*, 8858−8861. (m) Bouwkamp, M. W.; Lobkovsky, E.; Chirik, P. J. *J. Am. Chem. Soc.* **2005**, *127*, 9660−9661.

(10) (a) Ma, J.; Feng, C.; Wang, S.; Zhao, K.-Q.; Sun, W.-H.; Redshaw, C.; Soland, G. A. *Inorg. Chem. Front.* **2014**, *1*, 14−34 and references therein. (b) Lyaskovskyy, V.; de Bruin, B. *ACS Catal.* **2012**, *2*, 270−279. (c) Small, B. L.; Brookhart, M.; Bennett, A. M. A. *J. Am. Chem. Soc.* **1998**, *120*, 4049−4050. (d) Small, B. L.; Brookhart, M. *J. Am. Chem. Soc.* **1998**, *120*, 7143−7144. (e) Small, B. L.; Marcucci, A. J. *Organometallics* **2001**, *20*, 5738−5744. (f) Small, B. L. *Organometallics* **2003**, *22*, 3178−3183.

(11) (a) Campbell, N.; Henderson, A. W.; Taylor, D. *J. Chem. Soc.* **1953**, 1281−1285. (b) Joy, S. Ph.D. Thesis, Jadavpur University, Kolkata, India, 2012.

(12) Saha, A.; Das, C.; Goswami, S.; Peng, S.-M. *Indian J. Chem.* **2001**, *40A*, 198−201.

(13) Santra, B. K.; Thakur, G. A.; Ghosh, P.; Pramanik, A.; Lahiri, G. K. *Inorg. Chem.* **1996**, *35*, 3050−3052. (b) Kar, S.; Pradhan, B.; Sinha,

R. K.; Kundu, T.; Kodgire, P.; Rao, K. K.; Puranik, V. G.; Lahiri, G. K. *Dalton Trans.* **2004**, 1752−1760.
(14) Widger, L. R.; Jiang, Y.; Siegler, M. A.; Kumar, D.; Latifi, R.; de Visser, S. P.; Jameson, G. N. L.; Goldberg, D. P. *Inorg. Chem.* **2013**, *52*, 10467−10480.
(15) Sinan, M.; Panda, M.; Banerjee, P.; Shinisha, C. B.; Sunoj, R. B.; Goswami, S. *Org. Lett.* **2009**, *11*, 3218−3221.
(16) (a) Kaim, W. *Coord. Chem. Rev.* **1987**, *76*, 187−235. (b) Kaim, W. *Inorg. Chem.* **1984**, *23*, 3365−3368.
(17) Lesh, F. D.; Lord, R. L.; Heeg, M. J.; Bernhard, H. S.; Verani, C. N. *Eur. J. Inorg. Chem.* **2012**, 463−466.
(18) DFT analysis indicates charge delocalization between two coordinated ligands pointing to a formal charge of 0.5− for each ligand. However, a localized description with two different oxidation states, 1− and 0, is a more acceptable proposition, though such oxidation states are impossible[17] because the two resonating forms are isoenergetic.
(19) Goswami, S.; Mukherjee, R. N.; Chakravorty, A. *Inorg. Chem.* **1983**, *22*, 2825−2832.
(20) Available through http://ewww/mpi-heim.mpg.de/bac/logins/bill/julX_en.php.
(21) Sheldrick, G. M. *Acta Crystallogr., Sect. A* **1990**, *46*, 467−473.
(22) Sheldrick, G. M. *SHELXL 97, Program for the Refinement of Crystal Structures*; University of Göttingen, Göttingen, Germany, 1997.
(23) Frisch, M. J.; Trucks, G. W.; Schlegel, H. B.; Scuseria, G. E.; Robb, M. A.; Cheeseman, J. R.; Montgomery, J. A., Jr.; Vreven, T.; Kudin, K. N.; Burant, J. C.; Millam, J. M.; Iyengar, S. S.; Tomasi, J.; Barone, V.; Mennucci, B.; Cossi, M.; Scalmani, G.; Rega, N.; Petersson, G. A.; Nakatsuji, H.; Hada, M.; Ehara, M.; Toyota, K.; Fukuda, R.; Hasegawa, J.; Ishida, M.; Nakajima, T.; Honda, Y.; Kitao, O.; Nakai, H.; Klene, M.; Li, X.; Knox, J. E.; Hratchian, H. P.; Cross, J. B.; Bakken, V.; Adamo, C.; Jaramillo, J.; Gomperts, R.; Stratmann, R. E.; Yazyev, O.; Austin, A. J.; Cammi, R.; Pomelli, C.; Ochterski, J. W.; Ayala, P. Y.; Morokuma, K.; Voth, G. A.; Salvador, P.; Dannenberg, J. J.; Zakrzewski, V. G.; Dapprich, S.; Daniels, A. D.; Strain, M. C.; Farkas, O.; Malick, D. K.; Rabuck, A. D.; Raghavachari, K.; Foresman, J. B.; Ortiz, J. V.; Cui, Q.; Baboul, A. G.; Clifford, S.; Cioslowski, J.; Stefanov, B. B.; Liu, G.; Liashenko, A.; Piskorz, P.; Komaromi, I.; Martin, R. L.; Fox, D. J.; Keith, T.; Al-Laham, M. A.; Peng, C. Y.; Nanayakkara, A.; Challacombe, M.; Gill, P. M. W.; Johnson, B.; Chen, W.; Wong, M. W.; Gonzalez, C.; Pople, J. A. *Gaussian 09, Revision C.01*; Gaussian, Inc., Wallingford, CT, 2010.
(24) (a) Becke, A. D. *J. Chem. Phys.* **1993**, *98*, 5648−5652. (b) Lee, C.; Yang, W.; Parr, R. G. *Phys. Rev. B: Condens. Matter Mater. Phys.* **1988**, *37*, 785−789. (c) Vosko, S. H.; Wilk, L.; Nusair, M. *Can. J. Phys.* **1980**, *58*, 1200−1211. (d) Stephens, P. J.; Devlin, F. J.; Chabalowski, C. F.; Frisch, M. J. *J. Phys. Chem.* **1994**, *98*, 11623−11627.
(25) Schäfer, A.; Huber, C.; Ahlrichs, R. *J. Chem. Phys.* **1994**, *100*, 5829−5835.
(26) Ginsberg, A. P. *J. Am. Chem. Soc.* **1980**, *102*, 111−117.
(27) (a) Noodleman, L.; Case, D. A.; Aizman, A. *J. Am. Chem. Soc.* **1988**, *110*, 1001−1005. (b) Noodleman, L.; Davidson, E. R. *Chem. Phys.* **1986**, *109*, 131−143. (c) Noodleman, L.; Norman, J. G., Jr.; Osborne, J. H.; Aizman, C.; Case, D. A. *J. Am. Chem. Soc.* **1985**, *107*, 3418−3426. (d) Noodleman, L. *J. Chem. Phys.* **1981**, *74*, 5737−5743.
(28) Mulliken, R. S. *J. Chem. Phys.* **1955**, *23*, 1833−1840.
(29) (a) Bauernschmitt, R.; Ahlrichs, R. *Chem. Phys. Lett.* **1996**, *256*, 454−464. (b) Stratmann, R. E.; Scuseria, G. E.; Frisch, M. J. *J. Chem. Phys.* **1998**, *109*, 8218−8224. (c) Casida, M. E.; Jamoroski, C.; Casida, K. C.; Salahub, D. R. *J. Chem. Phys.* **1998**, *108*, 4439−4449.
(30) (a) Cossi, M.; Rega, N.; Scalmani, G.; Barone, V. *J. Comput. Chem.* **2003**, *24*, 669−681. (b) Cossi, M.; Barone, V. *J. Chem. Phys.* **2001**, *115*, 4708−4717. (c) Barone, V.; Cossi, M. *J. Phys. Chem. A* **1998**, *102*, 1995−2001. (d) O'Boyle, N. M.; Tenderholt, A. L.; Langner, K. M. *J. Comput. Chem.* **2008**, *29*, 839−845.
(31) Leininger, T.; Nicklass, A.; Stoll, H.; Dolg, M.; Schwerdtfeger, P. J. *J. Chem. Phys.* **1996**, *105*, 1052−1059.